applied optics

Numerical calculation of the mosaic error between mosaic gratings

Guojun Yang,[1,2] Xiangdong Qi,[1,*] Xiaotao Mi,[1] Shanwen Zhang,[1] Hongzhu Yu,[1] Haili Yu,[1] Xiaotian Li,[1] and Shuo Yang[1]

[1]Changchun Institute of Optics, Fine Mechanics and Physics, Chinese Academy of Sciences, Changchun, Jilin 130033, China
[2]University of Chinese Academy of Sciences, Beijing 100049, China
*Corresponding author: chinagrating@263.net.

Received 28 January 2020; revised 27 March 2020; accepted 2 April 2020; posted 3 April 2020 (Doc. ID 389274); published 30 April 2020

The theoretical calculation model for a mosaic error was established based on the plane equation for a grating surface and the relationship equation for a mosaic grating surface. A mosaic grating was obtained based on this model. In the experiment, the mosaic error was calculated based on the diffraction wavefronts of two groups of mosaic gratings that were obtained simultaneously with a Zygo interferometer. The difference between the wavefront of the mosaic grating and the average wavefront of the mosaic grating element was 0.031λ. The maximum far-field intensity of the mosaic grating was 90% of that without an error. This model provides a theoretical basis for the numerical mosaic between gratings. In addition, the mosaic error can be calculated with this model, and the quality of the mosaic grating can be evaluated.

https://doi.org/10.1364/AO.389274

1. INTRODUCTION

Diffraction gratings have been widely used as optical elements in various applications, including spectrometers [1–3], lasers [4–6], and couplers [7–9]. Large-size diffraction gratings are mainly used in astronomical spectrometers and laser systems for nuclear fusion [10–13]. In view of the difficulty of fabricating single large-size diffraction gratings, grating tiling is the main technique for fabricating large-size diffraction gratings.

Grating tiling technology involves placing two or more relatively small-sized gratings together and rectifying the mosaic errors between the mosaic gratings to meet certain tolerance requirements so that the mosaic gratings can be used as a single large-size grating. There are two methods for the correction of mosaic errors: direct correction and indirect correction. Direct correction mainly refers to calculating a mosaic error according to a theoretical model and adjusting the mosaic error through a mosaic device. Indirect correction mainly refers to adjusting a mosaic error based on the change of a far-field diffraction spot and a far-field interference fringe. Compared with indirect correction, direct correction has a higher correction accuracy and shorter correction time.

Early on, Qiao *et al.* [14], Harimoto [15], and Zeng and Li [16–18] corrected mosaic errors based on the indirect method. Prior to 2019, Cong *et al.* [19–21] established the theoretical calculation model of a mosaic error based on a three-dimensional space matrix and achieved the tiling of two echelle gratings based on the direct method. However, based on the theoretical calculation model, two optical paths with completely different structures needed to be built to obtain zero-order and non-zero-order diffraction wavefronts to calculate the mosaic error. This procedure is difficult to apply in engineering projects. Moreover, the zero-order diffraction light of an echelle grating is weak for a certain incident angle, so an interferometer cannot detect the zero-order diffraction wavefront. Therefore, the theoretical calculation model of a mosaic error needs further study to be more suitable for practical engineering applications.

In this study, based on the plane equation for a grating surface and the relationship equation for a mosaic grating surface, a theoretical calculation model for the mosaic error was established. A mosaic grating was obtained based on the theoretical calculation model of the mosaic error. In the experiment, the mosaic error was calculated based on the diffraction wavefronts of two groups of mosaic gratings that were obtained simultaneously with a Zygo interferometer. The diffraction wavefronts of two groups of mosaic gratings were obtained using only a structural optical path, which made the theoretical calculation model of the mosaic error more suitable for practical engineering applications. This model provides a theoretical basis for the numerical mosaic between gratings. In addition, the mosaic error can be calculated and the quality of mosaic grating can be evaluated by this model.

2. THEORETICAL CALCULATION MODEL FOR THE MOSAIC ERROR

A. Relationship Equation for the Mosaic Grating Surfaces

There were six dimensional errors between the mosaic gratings in this study, as shown in Fig. 1. The six dimensional mosaic errors are listed as follows: $\Delta\theta_x$, which was the error of rotation around the x axis (grating vector direction); $\Delta\theta_y$, which was the error of rotation around the y axis (grating line direction); $\Delta\theta_z$, which was the error of rotation around the z axis (grating normal direction); Δx, which was the error of translation along the x axis (grating vector direction); Δy, which was the error of translation along the y axis (grating line direction); and Δz, which was the error of translation along the z axis (grating normal direction). Among these errors, the translation error Δy only affected the effective area of the mosaic grating and did not affect the mosaic grating performance, so it could be ignored.

The grating surface could be regarded as the composition of n points numerically, and its surface could be represented by coordinates such as $[x_{1i}, y_{1i}, z_{1i}]$ and $[x_{2i}, y_{2i}, z_{2i}]$, where, $i = 1, 2, \ldots, n$. The origin of the coordinates was the center of the surface of the mosaic grating. According to the principle of three-dimensional coordinate transformation, the two coordinate systems of the mosaic grating surface could be completely coincident after rotation and translation. The relationship between the two surfaces of the mosaic grating can be expressed as

$$G_{2i}{}^T = R_z(\Delta\theta_z)\cdot R_y(\Delta\theta_y)\cdot R_x(\Delta\theta_x) \cdot \left\{ G_{1i}{}^T + \begin{bmatrix} \Delta x + L \\ \Delta y \\ \Delta z \end{bmatrix} \right\}, \tag{1}$$

where X^T represents the transpose of the matrix X. G_{1i} and G_{2i} represent any points on G_1 and G_2 gratings, respectively. L is the side length of the grating along the x direction. R_x, R_y, and R_z are the rotation matrices rotating around the x, y, and z axes, respectively, which can be obtained according to the rotation rule of space points around the coordinate axes [22]. Therefore, $R_x(\Delta\theta_x)$, $R_y(\Delta\theta_y)$, and $R_z(\Delta\theta_z)$ can be expressed as

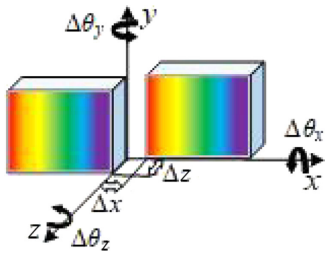

Fig. 1. Mosaic errors for the mosaic gratings. The x axis was parallel to the grating vector direction, the y axis was parallel to the grating line direction, and the z axis was parallel to the grating normal direction.

$$R_x(\Delta\theta_x) = \begin{bmatrix} 1 & 0 & 0 \\ 0 & \cos(\Delta\theta_x) & \sin(\Delta\theta_x) \\ 0 & -\sin(\Delta\theta_x) & \cos(\Delta\theta_x) \end{bmatrix}$$

$$R_y(\Delta\theta_y) = \begin{bmatrix} \cos(\Delta\theta_y) & 0 & -\sin(\Delta\theta_y) \\ 0 & 1 & 0 \\ \sin(\Delta\theta_y) & 0 & \cos(\Delta\theta_y) \end{bmatrix}. \tag{2}$$

$$R_z(\Delta\theta_z) = \begin{bmatrix} \cos(\Delta\theta_z) & \sin(\Delta\theta_z) & 0 \\ -\sin(\Delta\theta_z) & \cos(\Delta\theta_z) & 0 \\ 0 & 0 & 1 \end{bmatrix}$$

The two elements of the mosaic gratings were from the same master grating, and the grating surface could be regarded as completely consistent. Therefore, the overall surface coordinate of grating G_2 could be shifted to the G_1 direction by L. Then, Eq. (1) could be transformed as

$$G_{2i}{}^T = R_z(\Delta\theta_z)\cdot R_y(\Delta\theta_y)\cdot R_x(\Delta\theta_x)\cdot \left\{ G_{1i}{}^T + \begin{bmatrix} \Delta x \\ \Delta y \\ \Delta z \end{bmatrix} \right\}. \tag{3}$$

In the experiment with the grating tiling, the error of rotating was generally within 200 μrad, and the error of translation was generally within 2 μm. Therefore, the mosaic error could be regarded as a small amount. In addition, the z term in the equation represents the profile error of the grating surface. The profile error was the peak to valley (PV) of the grating surface, which was generally less than 0.25λ ($\lambda = 632.8$ nm) for a qualified grating, so z was also a small amount. According to the principle of small quantity approximation, the first-order small quantity was retained, and the second-order small quantity was ignored. By simplifying Eq. (3), the relationship equation between mosaic grating surfaces could be written as

$$\begin{bmatrix} x_{2i} \\ y_{2i} \\ z_{2i} \end{bmatrix} = \begin{bmatrix} x_{1i} + \Delta x + y_{1i}\cdot\Delta\theta_z \\ y_{1i} + \Delta y - x_{1i}\cdot\Delta\theta_z \\ z_{1i} + \Delta z + x_{1i}\cdot\Delta\theta_y - y_{1i}\cdot\Delta\theta_x \end{bmatrix}. \tag{4}$$

B. Plane Equation for the Grating Surface

The plane equation for the grating surface could be obtained from the plane fitting equation for the least squares method and the relationship between the grating surface and the diffraction wavefront. Based on the principle of the grating diffraction wavefront detected by the Zygo interferometer [23], the translation of the grating only affects the effective area of the diffraction wavefront detected. In addition, to facilitate the mosaic of gratings, the grating is usually adjusted to have only one-dimensional rotation error with the reference mirror before detecting the diffraction wavefront. Therefore, according to the principle that spatial two-point coordinates can be transformed into each other after rotation and translation, the geometric relationship between the coordinates of the points on the grating surface and the coordinates of the diffraction wavefront can be expressed as

$$\Delta^T = \left[R_y(\theta_i) + R_y(\theta_k)\right]\cdot G^T, \tag{5}$$

where θ_i is the incident angle, θ_k is the diffraction angle, $R_y(\theta_i)$ is the rotation matrix of the rotation θ_i angle around the y axis, $R_y(\theta_k)$ is the rotation matrix of the rotation θ_k angle around the y axis, G is the corresponding point of the grating surface, and Δ is the corresponding point of the diffraction wavefront. $\Delta = [u,\ v,\ w]$, where u and v are the pixels on the detector corresponding to the detected diffraction wavefront, and the units of u and v are one pixel. The detector in the Zygo interferometer has 512×480 pixels, and the size of a pixel is 18.512 μm. w is the wavefront of the grating, the measurement accuracy of which could reach 10^{-10} μm.

The numerical matrix of the diffraction wavefront obtained with the detector could be fitted into a plane based on the principle of least squares plane fitting. The plane fitting equation for the least squares method could be expressed as

$$w = a \cdot u + b \cdot v + c, \tag{6}$$

where a, b, and c are constants that represent the plane coefficients. a, b, and c could be determined according to the principle of the least squares method [24].

Therefore, by substituting Eq. (5) and grating equation Eq. (7) into Eq. (6), the plane equation for the grating surface could be obtained as shown in Eq. (8):

$$\sin\theta_i + \sin\theta_k = \frac{m\lambda}{d}, \tag{7}$$

where d is the grating constant, m is the diffraction order, and λ is the wavelength of the detection light:

$$\begin{aligned} z = &\frac{a \cdot (\cos\theta_i + \cos\theta_k) - \frac{m\lambda}{d}}{(\cos\theta_i + \cos\theta_k) + a \cdot \frac{m\lambda}{d}} \cdot x \\ &+ \frac{2b}{(\cos\theta_i + \cos\theta_k) + a \cdot \frac{m\lambda}{d}} \cdot y \\ &+ \frac{c}{(\cos\theta_i + \cos\theta_k) + a \cdot \frac{m\lambda}{d}}. \end{aligned} \tag{8}$$

C. Calculation of the Mosaic Error between the Mosaic Gratings

According to Eq. (8), the plane equation for the mosaic grating could be obtained as follows:

$$\begin{aligned} z_{1i} = &\frac{a_{11} \cdot (\cos\theta_i + \cos\theta_k) - \frac{m\lambda}{d}}{(\cos\theta_i + \cos\theta_k) + a_{11} \cdot \frac{m\lambda}{d}} \cdot x_{1i} \\ &+ \frac{2b_{11}}{(\cos\theta_i + \cos\theta_k) + a_{11} \cdot \frac{m\lambda}{d}} \cdot y_{1i} \\ &+ \frac{c_{11}}{(\cos\theta_i + \cos\theta_k) + a_{11} \cdot \frac{m\lambda}{d}}, \end{aligned} \tag{9}$$

$$\begin{aligned} z_{2i} = &\frac{a_{12} \cdot (\cos\theta_i + \cos\theta_k) - \frac{m\lambda}{d}}{(\cos\theta_i + \cos\theta_k) + a_{12} \cdot \frac{m\lambda}{d}} \cdot x_{2i} \\ &+ \frac{2b_{12}}{(\cos\theta_i + \cos\theta_k) + a_{12} \cdot \frac{m\lambda}{d}} \cdot y_{2i} \\ &+ \frac{c_{12}}{(\cos\theta_i + \cos\theta_k) + a_{12} \cdot \frac{m\lambda}{d}}, \end{aligned} \tag{10}$$

where a_{11}, b_{11}, and c_{11} are the coefficients of the plane equation for the G_1 surface; a_{12}, b_{12}, and c_{12} are the coefficients of the plane equation for the G_2 surface; d is the grating constant; m is the diffraction order; and λ is the wavelength of the detection light.

The displacement error in the y direction had no effect on the overall performance of the mosaic grating, such as dispersion, resolution, and wavefront, so it could be ignored. By substituting Eq. (4) into Eq. (10), another expression for the plane equation for the grating G_1 surface could be obtained, as shown in Eq. (11):

$$\begin{aligned} z_{1i} = &\frac{a_{12} \cdot (\cos\theta_i + \cos\theta_k) - \frac{m\lambda}{d} - \Delta\theta_y \cdot (\cos\theta_i + \cos\theta_k)}{(\cos\theta_i + \cos\theta_k) + a_{12} \cdot \frac{m\lambda}{d}} \cdot x_{1i} \\ &+ \frac{2b_{12} + \Delta\theta_x \cdot (\cos\theta_i + \cos\theta_k) - \Delta\theta_z \cdot \frac{m\lambda}{d}}{(\cos\theta_i + \cos\theta_k) + a_{12} \cdot \frac{m\lambda}{d}} \cdot y_{1i} \\ &+ \frac{c_{12} - \Delta x \cdot \frac{m\lambda}{d} - \Delta z \cdot (\cos\theta_i + \cos\theta_k)}{(\cos\theta_i + \cos\theta_k) + a_{12} \cdot \frac{m\lambda}{d}}. \end{aligned} \tag{11}$$

Based on the z axis, the corresponding coefficients of the two plane equations for the G_1 surfaces were equal. According to Eqs. (9) and (11), Eq. (12) could be obtained as follows:

$$\begin{aligned} &\frac{a_{12} \cdot (\cos\theta_i + \cos\theta_k) - \frac{m\lambda}{d} - \Delta\theta_y \cdot (\cos\theta_i + \cos\theta_k)}{(\cos\theta_i + \cos\theta_k) + a_{12} \cdot \frac{m\lambda}{d}} \\ &= \frac{a_{11} \cdot (\cos\theta_i + \cos\theta_k) - \frac{m\lambda}{d}}{(\cos\theta_i + \cos\theta_k) + a_{11} \cdot \frac{m\lambda}{d}}, \\ &\frac{2b_{12} + \Delta\theta_x \cdot (\cos\theta_i + \cos\theta_k) - \Delta\theta_z \cdot \frac{m\lambda}{d}}{(\cos\theta_i + \cos\theta_k) + a_{12} \cdot \frac{m\lambda}{d}} \\ &= \frac{2b_{11}}{(\cos\theta_i + \cos\theta_k) + a_{11} \cdot \frac{m\lambda}{d}}, \\ &\frac{c_{12} - \Delta x \cdot \frac{m\lambda}{d} - \Delta z \cdot (\cos\theta_i + \cos\theta_k)}{(\cos\theta_i + \cos\theta_k) + a_{12} \cdot \frac{m\lambda}{d}} \\ &= \frac{c_{11}}{(\cos\theta_i + \cos\theta_k) + a_{11} \cdot \frac{m\lambda}{d}}. \end{aligned} \tag{12}$$

Based on Eq. (12), $\Delta\theta_x$ and $\Delta\theta_z$ affected each other. $\Delta\theta_x$ and $\Delta\theta_z$ could not be calculated separately. Δx and Δz also affected each other, and Δx and Δz could not be calculated separately. However, the coefficients of $\Delta\theta_z$ and Δx were both $m\lambda/d$. Therefore, keeping the coefficients of $\Delta\theta_z$ and Δx unchanged, for another detection light with the same diffraction order and a different incident angle, another expression for the plane equation for the G_1 and G_2 surfaces could be obtained, and Eq. (13) could be obtained as follows:

$$\frac{a_{22}\cdot\left(\cos\theta_i'+\cos\theta_k'\right)-\frac{m\lambda}{d}-\Delta\theta_y\cdot\left(\cos\theta_i'+\cos\theta_k'\right)}{\left(\cos\theta_i'+\cos\theta_k'\right)+a_{22}\cdot\frac{m\lambda}{d}}$$

$$=\frac{a_{21}\cdot\left(\cos\theta_i'+\cos\theta_k'\right)-\frac{m\lambda}{d}}{\left(\cos\theta_i'+\cos\theta_k'\right)+a_{21}\cdot\frac{m\lambda}{d}},$$

$$\frac{2b_{22}+\Delta\theta_x\cdot\left(\cos\theta_i'+\cos\theta_k'\right)-\Delta\theta_z\cdot\frac{m\lambda}{d}}{\left(\cos\theta_i'+\cos\theta_k'\right)+a_{22}\cdot\frac{m\lambda}{d}}$$

$$=\frac{2b_{21}}{\left(\cos\theta_i'+\cos\theta_k'\right)+a_{21}\cdot\frac{m\lambda}{d}},$$

$$\frac{c_{22}-\Delta x\cdot\frac{m\lambda}{d}-\Delta z\cdot\left(\cos\theta_i'+\cos\theta_k'\right)}{\left(\cos\theta_i'+\cos\theta_k'\right)+a_{22}\cdot\frac{m\lambda}{d}}$$

$$=\frac{c_{21}}{\left(\cos\theta_i'+\cos\theta_k'\right)+a_{21}\cdot\frac{m\lambda}{d}},\tag{13}$$

where a_{21}, b_{21}, and c_{21} are the coefficients of the plane equation for the G_1 surface; a_{22}, b_{22}, and c_{22} are the coefficients of the plane equation for the G_2 surface; θ_i' is the incident angle; and θ_k' is the diffraction angle.

Therefore, according to Eqs. (12) and (13), the mosaic errors could be calculated as follows:

$$\begin{cases}\Delta\theta_x=\dfrac{\frac{2b_{21}\cdot[\left(\cos\theta_i'+\cos\theta_k'\right)+a_{22}\cdot\frac{m\lambda}{d}]}{\left(\cos\theta_i'+\cos\theta_k'\right)+a_{21}\cdot\frac{m\lambda}{d}}-\frac{2b_{11}\cdot[(\cos\theta_i+\cos\theta_k)+a_{12}\cdot\frac{m\lambda}{d}]}{(\cos\theta_i+\cos\theta_k)+a_{11}\cdot\frac{m\lambda}{d}}-(2b_{22}-2b_{12})}{\left(\cos\theta_i'+\cos\theta_k'\right)-(\cos\theta_i+\cos\theta_k)}\\ \Delta\theta_y=-\dfrac{\frac{a_{11}\cdot(\cos\theta_i+\cos\theta_k)-\frac{m\lambda}{d}}{(\cos\theta_i+\cos\theta_k)+a_{11}\cdot\frac{m\lambda}{d}}\cdot[(\cos\theta_i+\cos\theta_k)+a_{12}\cdot\frac{m\lambda}{d}]-a_{12}\cdot(\cos\theta_i+\cos\theta_k)+\frac{m\lambda}{d}}{(\cos\theta_i+\cos\theta_k)}\\ \Delta\theta_z=\dfrac{2b_{12}+\Delta\theta_x\cdot(\cos\theta_i+\cos\theta_k)}{\frac{m\lambda}{d}}-\dfrac{2b_{11}\cdot\left[(\cos\theta_i+\cos\theta_k)+a_{12}\cdot\frac{m\lambda}{d}\right]}{(\cos\theta_i+\cos\theta_k)\cdot\frac{m\lambda}{d}+a_{11}\cdot\left(\frac{m\lambda}{d}\right)^2}\\ \Delta z=-\dfrac{\frac{c_{21}\cdot\left[\left(\cos\theta_i'+\cos\theta_k'\right)+a_{22}\cdot\frac{m\lambda}{d}\right]}{\left(\cos\theta_i'+\cos\theta_k'\right)+a_{21}\cdot\frac{m\lambda}{d}}-\frac{c_{11}\cdot[(\cos\theta_i+\cos\theta_k)+a_{12}\cdot\frac{m\lambda}{d}]}{(\cos\theta_i+\cos\theta_k)+a_{11}\cdot\frac{m\lambda}{d}}-(c_{22}-c_{12})}{\left(\cos\theta_i'+\cos\theta_k'\right)-(\cos\theta_i+\cos\theta_k)}\\ \Delta x=\dfrac{c_{12}-\Delta z\cdot(\cos\theta_i+\cos\theta_k)}{\frac{m\lambda}{d}}-\dfrac{c_{11}\cdot\left[(\cos\theta_i+\cos\theta_k)+a_{12}\cdot\frac{m\lambda}{d}\right]}{(\cos\theta_i+\cos\theta_k)\cdot\frac{m\lambda}{d}+a_{11}\cdot\left(\frac{m\lambda}{d}\right)^2}\end{cases}.\tag{14}$$

3. EXPERIMENT

A. Wavefront Detection System for a Mosaic Grating

Figure 2 shows the experimental optical path diagram of the wavefront detection system for the mosaic grating. As shown in Fig. 2, a Zygo interferometer was used to detect the wavefronts of the mosaic gratings. A prism was used to generate a second incident angle for the detection beam in the same error detection optical path. Mirrors 1 and 2 were used to make the two incident angle detection beams return to their original path after grating diffraction to allow the Zygo interferometer to detect the grating wavefront. The key parameters for all of the components are listed in Table 1. In the experiment, the first incident angle θ_i was 68°, the first diffraction angle θ_k was 60.75°, the second incident angle θ_i' was 74.66°, and the second diffraction angle θ_k' was 56.65°. In addition, the blaze order of grating is −36th, which is usually selected as the mosaic order.

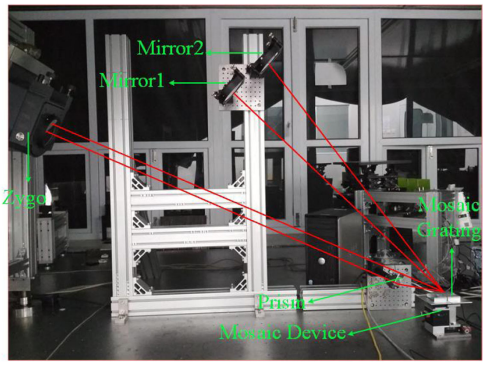

Fig. 2. Experimental optical path diagram of the wavefront detection system for the mosaic grating.

B. Mosaic Device

The mosaic device consisted of three rotating tables controlled by the actuator and two piezoelectric ceramic translation tables, as shown in Fig. 3 . The rotation of the rotary table was achieved by adjusting the step number of the actuator. The translation of the translation table was achieved by adjusting the step number of the piezoelectric ceramics. The detailed adjustment parameters for the correction of the mosaic errors with this device are listed in Table 2.

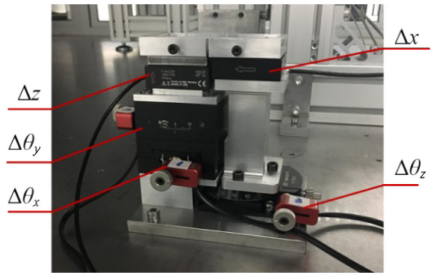

Fig. 3. Mechanical structure of the mosaic device.

Table 1. Key Parameters for All Components

Components	Parameters	Performance Index
Zygo interferometer	Wavelength	632.8 nm
	Beam diameter	100 mm
	Type	GPI XP/D
Mirror	Diameter	100 mm
	Reflectivity	>90%
	PV	$0.05\lambda(\lambda = 632.8\ \text{nm})$
Prism	Material	Quartz
	Pass light area	50 mm × 50 mm
	Wedge angle	14°
Mosaic grating element	Area	35 mm × 35 mm
	Groove density	79 line/mm
	Blaze angle	64°
Mosaic device	Rotation accuracy	0.3 μrad
	Translation accuracy	1 nm

Table 2. Parameters of the Adjustment Mechanisms Used for the Correcting Errors

Mosaic Errors	$\Delta\theta_x$	$\Delta\theta_y$	$\Delta\theta_z$	Δx	Δz
Step (nm)	30	30	30	1	1
Rotation radius (mm)	100	70	65	—	—
Trip	12.7 mm	12.7 mm	12.7 mm	250 μm	250 μm
Step angle (μrad)	0.300	0.429	0.462	—	—
Step number	$\Delta\theta_x/0.3$	$\Delta\theta_y/0.429$	$\Delta\theta_z/0.462$	$\Delta x/1$	$\Delta z/1$

4. RESULTS AND DISCUSSION

The correction of the mosaic error included rough correction and fine correction. The rough correction involved adjusting the far-field spot coincidence of the mosaic grating. The fine correction involved adjusting the size of the mosaic error to meet the requirements. In the experiment, after rough correction, the −36th diffraction wavefront obtained with the Zygo interferometer for the mosaic grating was as shown in Fig. 4. There were two groups of wavefronts for the mosaic grating, as shown in Fig. 4. The wavefront of the upper two gratings was the diffraction wavefront at the first incident angle, and the wavefront of the lower two gratings was the diffraction wavefront at the second incident angle. The wavefronts of the first and third gratings are the wavefronts of the reference gratings, and the wavefronts of second and fourth gratings are the wavefronts of the adjusting gratings. According to the principle of the least

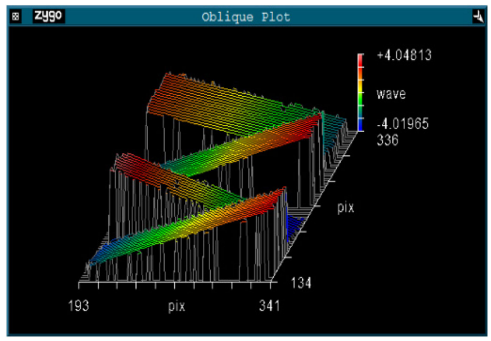

Fig. 4. −36th diffraction wavefront for the mosaic grating obtained with the Zygo interferometer at two incident angles.

Table 4. Adjustment Steps of the Actuator and the Piezoelectric Ceramic for the Correcting Errors

Mosaic Errors	$\Delta\theta_x$	$\Delta\theta_y$	$\Delta\theta_z$	Δx	Δz
Step number	150	430	50	176	316

squares method, the plane fitting coefficients of the four wavefronts in Fig. 4 could be obtained as shown in Table 3. Then, the errors between the mosaic gratings in Fig. 4 could be calculated by Eq. (14) as shown in Eq. (15):

$$\begin{cases} \Delta\theta_x = 44.865\ \mu\text{rad} \\ \Delta\theta_y = 184.39\ \mu\text{rad} \\ \Delta\theta_z = 23.275\ \mu\text{rad} \\ \Delta z = 175.87\ \text{nm} \\ \Delta x = 315.97\ \text{nm} \end{cases}. \tag{15}$$

Based on the mechanical adjustment parameters in Table 2, the step numbers of the actuator and the piezoelectric ceramic could be calculated as shown in Table 4. Therefore, in the same calculation process as Eq. (15), after the fine correction process from the diffraction wavefront in Fig. 4 to the diffraction wavefront in Fig. 5(a), the errors between the mosaic gratings in Fig. 5(a) could be calculated as

$$\begin{cases} \Delta\theta_x = 0.822\ \mu\text{rad} \\ \Delta\theta_y = 0.253\ \mu\text{rad} \\ \Delta\theta_z = 0.576\ \mu\text{rad} \\ \Delta z = 8.745\ \text{nm} \\ \Delta x = 17.105\ \text{nm} \end{cases}, \tag{16}$$

where Fig. 5(a) shows the −36th diffraction wavefront for the mosaic grating obtained by the Zygo interferometer after fine correction, and Table 5 shows the plane fitting coefficients of the four wavefronts in Fig. 5(a).

Table 3. Plane Fitting Coefficients of the Four Wavefronts

First Incident Angle		Second Incident Angle	
Wavefront1	Wavefront2	Wavefront1	Wavefront2
$a_{11} = -4.9411 \times 10^{-5}$	$a_{12} = -1.4919 \times 10^{-5}$	$a_{21} = -8.7551 \times 10^{-5}$	$a_{22} = -4.4425 \times 10^{-5}$
$b_{11} = -8.0342 \times 10^{-6}$	$b_{12} = -6.4541 \times 10^{-6}$	$b_{21} = 3.4163 \times 10^{-7}$	$b_{22} = 3.0188 \times 10^{-6}$
$c_{11} = 6.7847 \times 10^{-8}$	$c_{12} = 2.4079 \times 10^{-8}$	$c_{21} = 1.0109 \times 10^{-7}$	$c_{22} = 4.1856 \times 10^{-8}$

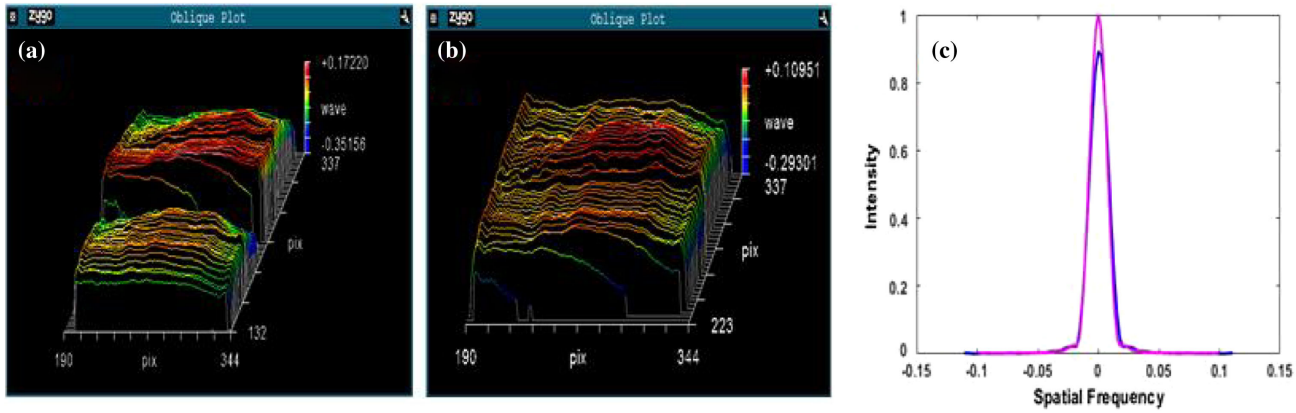

Fig. 5. (a) −36th diffraction wavefront for the mosaic grating obtained with the Zygo interferometer at two incident angles after fine correction. (b) −36th diffraction wavefront of the mosaic grating at one of the two incident angles. (c) Far-field energy distribution for the mosaic grating. The pink curve indicates the situation when the error was zero and the blue curve indicates the situation when $\Delta\theta_x = 0.822$ μrad, $\Delta\theta_y = 0.253$ μrad, $\Delta\theta_z = 0.576$ μrad, $\Delta z = 8.745$ nm, and $\Delta x = 17.105$ nm.

Table 5. Plane Fitting Coefficients of the Four Wavefronts

First Incident Angle		Second Incident Angle	
Wavefront1	**Wavefront2**	**Wavefront1**	**Wavefront2**
$a_{11} = 1.6708 \times 10^{-5}$	$a_{12} = 1.6756 \times 10^{--5}$	$a_{21} = 1.6386 \times 10^{-5}$	$a_{22} = 1.6250 \times 10^{-5}$
$b_{11} = -2.7606 \times 10^{-7}$	$b_{12} = -1.1491 \times 10^{-6}$	$b_{21} = -1.6521 \times 10^{-6}$	$b_{22} = -2.5050 \times 10^{-6}$
$c_{11} = -1.6194 \times 10^{-8}$	$c_{12} = -1.5222 \times 10^{-8}$	$c_{21} = -1.7349 \times 10^{-8}$	$c_{22} = -1.5539 \times 10^{-8}$

The diffraction wavefront of mosaic grating can be characterized only by the wavefront at an incident angle. Therefore, Fig. 5(b) was obtained. Figure 5(b) shows the −36th diffraction wavefront of the mosaic grating at one of the two incident angles. The PV was 0.403λ. In the experiment, the PV wavefronts of the mosaic grating elements were 0.349λ and 0.395λ. The average PV wavefront of the mosaic grating element was 0.372λ. The difference between the mosaic grating wavefront and the average wavefront of the mosaic grating element (ΔPV) was 0.031λ. In the experiment, when the value of ΔPV was less than 0.2λ, we considered that the grating had been perfectly mosaicked. Therefore, the PV wavefront of the mosaic grating met the requirement. In addition, except for the wavefront of the mosaic grating, the far-field energy of the mosaic grating could also be used to evaluate the quality of the mosaic grating. As shown in Fig. 5(c), based on Fraunhofer's principle [25], the far-field energy distribution of the mosaic grating was obtained with MATLAB. The maximum far-field diffraction intensity of the mosaic grating was 90% of that without an error, which met the requirement that the maximum far-field diffraction intensity of the mosaic grating was 90% of that without an error.

5. CONCLUSION

The theoretical calculation model of a mosaic error was established based on the plane equation for a grating surface and the relationship equation for a mosaic grating surface. Based on this model, we determined the mosaic of two echelle gratings. In the experiment, the mosaic error was calculated based on the diffraction wavefront of two groups of mosaic gratings that were obtained simultaneously with a Zygo interferometer. The difference between the wavefront of the mosaic grating and the average wavefront of the mosaic grating element (ΔPV) was 0.031λ. The maximum far-field diffraction intensity of the mosaic grating was 90% of that without an error. These two results proved the effectiveness of the theory calculation model for the mosaic error. Compared with the previous theoretical calculation model for a mosaic error, this model only needed to build an optical path with a structure to obtain two groups of wavefronts for the mosaic grating for error calculation, which made this theoretical calculation model more suitable for practical engineering applications. This model is suitable for all blazed gratings with different line densities and different blazed angles, and this model provides a theoretical basis for the numerical mosaic between gratings. In addition, a mosaic error can be calculated with this model, and the quality of a mosaic grating can be evaluated.

Funding. National Key Research and Development Program of China (2016YFF0102006); National Natural Science Foundation of China (61975255, 61605204, 61505204); National Youth Program Foundation of China (61805233); Jilin Province Key Technology Project in China (20190302047GX).

Disclosures. The authors declare no conflicts of interest.

REFERENCES

1. J. J. Talghader, A. S. Gawarikar, and R. P. Shea, "Spectral selectivity in infrared thermal detection," Light Sci. Appl. **1**, e24 (2012).
2. J. Reimers, A. Bauer, K. Thompson, and J. Rolland, "Freedom spectrometer enabling increased compactness," Light Sci. Appl. **6**, 1–10 (2017).

3. J. Qiu, X. Qi, X. Li, Y. Tang, J. Lantu, X. Mi, and H. Bayan, "Broadband transmission Raman measurements using a field-widened spatial heterodyne Raman spectrometer with mosaic grating structure," Opt. Express **26**, 26106–26119 (2018).
4. S. Breitkopf, T. Eidam, A. Klenke, L. Von, H. Carstens, S. Holzberger, E. Fill, T. Schreiber, F. Krausz, A. Tunnermann, I. Pupeza, and J. Limpert, "A concept for multiterawatt fibre lasers based on coherent pulse stacking in passive cavities," Light Sci. Appl. **3**, e211 (2014).
5. O. Mhibik, S. Forget, D. Ott, G. Venus, I. Divliansky, L. Glebov, and S. Chenais, "An ultra-narrow linewidth solution-processed organic laser," Light Sci. Appl. **5**, e16026 (2016).
6. N. Blanchot, E. Bar, G. Behar, C. Bellet, D. Bigourd, F. Boubault, C. Chappuis, H. Coic, C. Damiens-Dupont, O. Flour, O. Hartmann, L. Hilsz, E. Hugonnot, E. Lavastre, J. Luce, E. Mazataud, J. Neauport, S. Noailles, B. Remy, F. Sautarel, M. Sautet, and C. Rouyer, "Experimental demonstration of a synthetic aperture compression scheme for multi-petawatt high-energy lasers," Opt. Express **18**, 10088–10097 (2010).
7. M. Schumann, T. Biiclunann, N. Gruhler, M. Wegener, and W. Pernice, "Hybrid 2D–3D optical devices for integrated optics by direct laser writing," Light Sci. Appl. **3**, e175 (2014).
8. S. Logan, T. Rahul, N. V. Sapra, A. Y. Piggot, D. Vercruysse, and J. Vuckovic, "Fully-automated optimization of grating couplers," Opt. Express **26**, 4023–4034 (2018).
9. M. G. Sabor, Y. Wang, E. El-Fiky, D. Patel, A. K. Shahriar, M. S. Alam, M. Jacques, Z. P. Xing, L. H. Xu, N. Abadia, and D. Plant, "Transversely coupled Fabry–Perot resonators with Bragg grating reflectors," Opt. Lett. **43**, 13–16 (2018).
10. A. Szentgyorgyi, D. Baldwin, S. Barnes, J. Bean, S. Ben-Ami, P. Brennan, J. Budynkiewicz, M. Y. Chun, C. Conroy, J. D. Crane, H. Epps, I. Evans, J. Evans, J. Foster, A. Frebel, T. Gauron, D. Guzmán, T. Hare, B. H. Jang, J. G. Jang, A. Jordan, J. Kim, K. M. Kim, C. M. M. Oliveira, M. Lopez-Morales, K. McCracken, S. McMuldroch, J. Miller, M. Mueller, J. S. Oh, C. Onyuksel, M. Ordway, B. G. Park, C. Park, S. J. Park, C. Paxson, D. Phillips, D. Plummer, W. Podgorski, A. Seifahrt, D. Stark, J. Steiner, A. Uomoto, R. Walsworth, and Y. S. Yu, "The GMT-Consortium Large Earth Finder (G-CLEF): An optical echelle spectrograph for the Giant Magellan Telescope (GMT)," Proc. SPIE **9908**, 990822 (2016).
11. J. L. Lizon, H. Dekker, A. Manescau, D. Megevan, F. A. Pepe, and M. Riva, "A large mosaic echelle grating for ESPRESSO spectrograph," Proc. SPIE **10701**, 107012P (2018).
12. D. N. Maywar, J. H. Kelly, L. J. Waxer, S. F. B. Morse, I. A. Begishev, J. Bromage, C. Dorrer, J. L. Edwards, L. Folnsbee, M. J. Guardalben, S. D. Jacobs, R. Jungquist, T. J. Kessler, R. W. Kidder, B. E. Kruschwitz, S. J. Loucks, J. R. Marciante, R. L. McCrory, D. D. Meyerhofer, A. V. Okishev, J. B. Oliver, G. Pien, J. Qiao, J. Puth, A. L. Rigatti, A. W. Schmid, M. J. Shoup, III, C. Stoeckl, K. A. Thorp, and J. D. Zuegel, "OMEGA EP high-energy petawatt laser: Progress and prospects," J. Phys. Conf. Ser. **112**, 32007 (2008).
13. J. Neauport and N. Bonod, "Pulse compression gratings for the PETAL project: A review of various technologies," Proc. SPIE **7132**, 71320D (2009).
14. J. Qiao, A. Kalb, M. Guardalben, G. King, D. Canning, and J. H. Kelly, "Large-aperture grating tiling by interferometry for petawatt chirped-pulse–amplification systems," Opt. Express **15**, 9562–9574 (2007).
15. T. Harimoto, "Far-field pattern analysis for an array grating compressor," Jpn. J. Appl. Phys. **43**, 1362–1365 (2004).
16. L. J. Zeng and L. F. Li, "Method of making mosaic gratings by using a two-color heterodyne interferometer containing a reference grating," Opt. Lett. **31**, 152–154 (2006).
17. Y. Hu, L. J. Zeng, and L. F. Li, "Method to mosaic gratings that relies on analysis of far-field intensity patterns in two wavelengths," Opt. Commun. **269**, 285–290 (2007).
18. Y. Hu and L. J. Zeng, "Grating mosaic based on image processing of far-field diffraction intensity patterns in two wavelengths," Appl. Opt. **46**, 7018–7025 (2007).
19. M. Cong, X. D. Qi, X. T. Mi, and H. Bayan, "Interference method for mosaicking echelles using double-angle incident light and a mirror-echelle structure," Opt. Eng. **57**, 064111 (2018).
20. M. Cong, X. D. Qi, J. Xu, C. Qiao, X. T. Mi, X. T. Li, H. L. Yu, S. W. Zhang, H. Z. Yu, and H. S. G. Bayan, "Analysis and removal of five-dimensional mosaicking errors in mosaic grating," Opt. Express **27**, 1968–1980 (2019).
21. M. Cong, X. D. Qi, X. T. Mi, X. T. Li, H. L. Yu, S. W. Zhang, H. Z. Yu, and H. S. G. Bayan, "Concurrent monitoring of zeroth-order and diffraction-order interference fringes for mosaicking echelle," Opt. Commun. **435**, 271–276 (2019).
22. X. G. Xu, "Research on workspace of rotary table machine tools based on homogeneous coordinate transformation matrix," Sci. Technol. Inf. **13**, 94–95 (2013).
23. L. Y. Qian, Y. S. Huang, D. W. Zhang, Z. J. Ni, and S. L. Zhuang, "Wavefront measurement of diffraction grating based on laser interferometer," Opto-Electron. Eng. **40**, 67–74 (2013).
24. X. C. Huo and X. P. Li, "Fitting surface equation with least square method," J. Chifeng Univ. Nat. Sci. Ed. **6**, 17–19 (2009).
25. X. Y. Lu, X. D. Qi, H. L. Yu, X. T. Li, S. W. Zhang, S. Jiang, and L. Yin, "Precision analysis of grating replicated mosaic error based on the principle of Fraunhofer," Chin. J. Lasers **43**, 0508005 (2016).